sustainability

MDPI

Article

Evolution Law of Micro-Pore Structure of Cement-Emulsified Asphalt Mortar Based on NMR

Shanshan Jin *, Weinan Zhan and Yang Zhang

Beijing Urban Transportation Infrastructure Engineering Technology Research Center, Beijing University of Civil Engineering and Architecture, Beijing 100044, China
* Correspondence: jinshanshan@bucea.edu.cn

Abstract: Cement emulsified asphalt mortar (CA) is widely used as the cushion of two types of ballastless track (CRTS I and CRTS II) in high-speed railways. Nowadays, the lack of durability of CA mortar has severely affected the quality of high-speed railways, failing to meet the requirements of sustainability. Since CA mortar is a kind of porous material, its performance can be significantly affected by its microstructures, which means that revealing the evolution law of its microstructures can provide the basis for improving its durability. Therefore, CA mortar species with different asphalt-cement ratio under different curing ages were prepared based on the requirements of CRTS II in this research and the pore structures were determined based on SEM and NMR methods. Then, a fractal model of CA mortar pore volume was proposed based on the concept of box fractal dimension, and the fractal dimension of pore volume was calculated. The relationship between fractal dimensions and mechanical property was analyzed based on Pearson correlation coefficient and regression analysis. The results suggested that the overall microstructure of CA mortar shows a loose porous space structure with cement hydration products being the continuous phase and asphalt being the dispersed phase. With the increase in A/C ratio, the hydration products produced by cement hydration decrease, and the total porosity and average porosity of CA mortar gradually increase due to the increase of asphalt hindering the hydration process of the cement. With the increase in curing age, the pore structure of CA mortar becomes more compact. However, the evolution law of CA mortar pore structure with age is not consistent under different A/C ratios due to the influence of asphalt. The pore structure of CA mortar was proved to have obvious fractal characteristics based on the concept of box fractal dimension and the experimental data of NMR. In addition, the correlation analysis proves that the fractal dimension of pore structure has an obvious positive correlation with the compressive and flexural strength, which suggests that the fractal dimension of pore volume can be a bridge for connecting the macro-property and micro-structures of CA mortar.

Keywords: cement-emulsified asphalt mortar; pore structure; SEM; NMR; fractal model; fractal dimension

Citation: Jin, S.; Zhan, W.; Zhang, Y. Evolution Law of Micro-Pore Structure of Cement-Emulsified Asphalt Mortar Based on NMR. *Sustainability* **2022**, *14*, 15508. https://doi.org/10.3390/su142315508

Academic Editors: Boshan Chen, Beibei Li, Lulu Zhang, Letian Hai, Quanxi Ye and Zhiyuan Fang

Received: 15 October 2022
Accepted: 8 November 2022
Published: 22 November 2022

1. Introduction

CA mortar is mainly used for the high-speed rail ballastless track cushion. Some diseases like cracking, peeling, pulping, and interface separation between the track slab and the base slab are commonly witnessed during the use process, which reduces both the performance and service life of CA mortar causing it to fail to meet the requirement of sustainability. Cement-emulsified asphalt (CA) mortar is a kind of cement-based porous material, whose microstructure determines its macro-properties. The pore structure is an important part of the material microstructure, which has an important influence on the macro-properties, such as permeability resistance, frost resistance, thermal conductivity, water absorption and strength [1]. Given the above problems, it is of significance to study the mechanism of macro-properties from a microscopic angle for improving the macro-properties. With the addition of asphalt, the mortar structure becomes more complex, making the testing and analysis of the microstructure of CA mortar more difficult. Kong

X.M. et al. argued that emulsified asphalt will prolong the cement hydration induction period, and asphalt particles adsorbed on the surface of cement particles hinder the contact between water and cement, thus delaying cement hydration [2]. Li W. et al. studied the influence of the presence or absence of emulsified asphalt on the CA mortar microstructure via mercury intrusion porosimetry (MIP), and found that the emulsified asphalt inhibits the cement hydration, gradually weakening its mechanical properties [3]. It can be seen that asphalt has a significant impact on the micro-pore structure of CA mortar. However, few research results do not form a system, and no consensus has been reached. Therefore, it is necessary to study and analyze the micro-pore structure of CA mortar and its evolution law.

Currently, many measurement methods for the microstructure of cement-based materials such as constant temperature and humidity drying method (CTHD), MIP and environmental scanning electron microscopy (SEM) can be used to accurately detect the interconnected pore structure of CA mortar, but they all have some deficiencies. CTHD can be used to accurately measure the interconnected pore porosity of CA mortar but cannot measure the continuous pore size distribution [4], and the test process is so complicated that the test results will be easily affected. MIP can be used for the pore structure analysis of cement-based materials during hydration, but the test process will cause damage to the sample, and the measurement error of the pore structure of low-strength CA mortar is larger [5]. SEM can directly measure the micro-pore morphology of cement-based materials, and more conveniently distinguish hydration products, but it fails to quantify the porosity and pore size distribution.

In recent years, nuclear magnetic resonance (NMR), an emerging microstructure test method characterized by rapidness, continuity and non-invasion, has been gradually introduced to the determination of the pore structure of CA mortar [6]. Deng D.H. et al. compared MIP, CTHD and NMR in the test of the pore structure of CA mortar, and found that NMR can measure the pore size distribution and porosity of interconnected pores inside the CA mortar more accurately than other methods [4]. Following asphalt extraction and filtration, Liu Z.Q. et al. analyzed the micro-pore structure changes in CA mortar and the influence of cement hydration degree on the long-term mechanical properties of mortar through MIP and NMR. The results showed that with continuous cement hydration, the pore structure of CA mortar is gradually refined, and the mechanical properties are continuously enhanced [7].

In this paper, the microscopic pore structure of CA mortar was measured and analyzed by the SEM and NMR method. A pore volume fractal model was established to calculate the fractal dimension of the pore structure of CA mortar. Then, both the evolution law of the microscopic pore structure of CA mortar and the relationship between flexural and compressive strength and pore volume fractal dimension were revealed to provide an experimental and theoretical basis for studying the relationship between microstructure and macro-properties, which is the research foundation for increasing the service life of CA mortar and creating considerable social and economic benefits.

2. Objective and Scope

Three kinds of CA mortars with different asphalt/cement (A/C) ratios were designed, their pore structure morphology and topography were photographed by SEM, and their microstructure was visually characterized. Meanwhile, the micro-pore structure of CA mortar was continuously measured by low-field NMR. The pore structure of CA mortar was qualitatively and quantitatively analyzed by combining the two test results. The pore volume fractal model was established based on the definition of box dimension, and the pore volume fractal dimension was calculated. Then, the evolution law of the pore structure of CA mortar was revealed, and the relationship between the compressive and flexural strength and the pore volume fractal dimension was established. The findings lay a foundation for guiding the optimization of macro-properties from a microscopic angle.

3. Materials and Experimental Design

3.1. Raw Materials

Ordinary Portland cement 42.5 was used, with a density of 3.15 g/cm^3. Machine-made silica sand was used as the standard sand, with a fineness modulus of 2.58, a maximum particle size of 2.50 mm, and a density of 2.64 g/cm^3. Anionic slow-breaking emulsified asphalt emulsified by JY-A3T1 anionic emulsifier was adopted in this research, with penetration of 7 mm, softening point at 48 °C and solid asphalt content of 60%. Tap water was adopted as mixing water. Polycarboxylic acid high-performance water-reducing agents were adopted, with a water-reducing rate of 25%. Scaly aluminum powder with a particle size of 50–75 μm was used. UEA expanding agents and organic silicon defoaming agents were used.

3.2. Mix Proportions

The mix proportions in this research were designed based on the standard of Temporary Technical Conditions for Cement Emulsified Asphalt Mortar for CRTS II Slab Ballastless Track of Passenger Dedicated Railway [8], which requires that the A/C ratio of CA mortar should be above 0.35, and the water-cement ratio should be under 0.58 for a suitable workability performance and strength. Therefore, 3 kinds of CA mortar with different A/C ratio (0.4, 0.5 and 0.6) were designed as shown in Table 1. The water-cement ratio was 0.48 and the dosage of the water-reducing agent was 0.5% in all tests.

Table 1. Mix proportions.

Number	W/C	A/C	Emulsified Asphalt/(kg/m^3)	Cement/(kg/m^3)	Sand/(kg/m^3)	Water/(kg/m^3)	Expanding Agents/(kg/m^3)
1	0.48	0.4	225	563	867	185	28
2	0.48	0.5	263	526	867	153	25
3	0.48	0.6	296	493	867	124	22

3.3. Preparation Methods

The raw materials were weighed according to the mix proportions established. The additive water and emulsified asphalt were placed into an agitator kettle, stirred at a low speed for 30 s, added with the uniformly-stirred dry materials, and stirred at a low speed for another 30 s, during which the polycarboxylic acid water reducing agent and organic silicon defoaming agent were added, followed by stirring at a high speed for 120 s. Finally, the mixture was stirred again at a low speed for 30 s. Following the "Interim Technical Conditions for Cement-Emulsified Asphalt Mortar for Passenger Dedicated Railway CRTS II Slab Ballastless Track", a workability test was conducted on the newly-mixed CA mortar, controlling the fluidity and expansion degree at 80–120 s and <16 s, respectively. Then, the newly-mixed CA mortar was prepared into samples (40 mm × 40 mm × 160 mm), demolded and cured in a standard curing room till a specified curing age.

3.4. Test Methods

3.4.1. SEM

A HITACHI SU8010 environmental SEM was used. The test sample (about 1 cm × 1 cm × 1 cm) was sprayed with gold on the surface to improve the conductivity. The SEM temperature was 20 °C, and the curing ages were 7 d, 14 d and 28 d.

3.4.2. Pore Structure Test

A MesoMR23-060H low-field NMR imaging analyzer was used, with a permanent magnet, a resonance frequency of 23.403 MHz, a magnet temperature at (32.00 ± 0.02) °C, and the maximum diameter of the probe coil of 60 mm. The test sample (40 mm × 40 mm × 80 mm) was cut from the 40 mm × 40 mm × 160 mm sample at a specified curing age.

3.4.3. Compressive and Flexural Strength Test

The compressive and flexural strength of CA mortar is determined based on the standard Method of Testing Cements-Determination of Strength (GB/T17671-2021) [9]. During the test process, the flexural strength is first tested by the TYE-300D flexural and compressive testing machine of cement mortar at a rate of 50N/S10N/S until the prism is broken. Then, the compressive strength of CA mortar is tested at a speed of 2400N/S using the two halves of specimens left in the flexural strength test.

3.4.4. Processing Method of NMR Data

According to the NMR relaxation mechanism, when the external magnetic field is not too strong or the echo interval is short enough, the transverse relaxation time (T_2) of the CA mortar sample without large pores is mainly affected by the surface fluid relaxation [10–13]. T_2 can be determined by the specific surface area of the channel, so T_2 can be expressed as:

$$\frac{1}{T_2} \approx \frac{1}{T_{2surf}} = \frac{S}{V_P}\rho \tag{1}$$

in which, ρ: the relaxation rate; S: the total surface area of pores; V_P: the total volume of pores.

The relationship between S/V and the pore radius r can be expressed as:

$$\frac{S}{V_P} = \frac{F_S}{r} \tag{2}$$

In the formula, F_S is the geometric shape factor, and F_S is usually taken as 2 for the columnar pores of the CA mortar, so that the relationship between the pore radius and relaxation time can be obtained as Equation (3):

$$r = \rho T_2 F_S \tag{3}$$

It can be seen from the literature that the spectral area of the T_2 energy spectrum curve is proportional to the amount of fluid contained in the CA mortar after water retention [14], so the spectral area is related to the porosity of the CA mortar. Therefore, by measuring the T_2 energy spectrum curve of the CA mortar sample before and after drying for many times, the relationship between the energy spectrum signal intensity and porosity can be obtained by the difference between the quality of the CA mortar sample and the difference between the energy spectrum area. Therefore, the relationships between the energy spectrum signal intensity and porosity under each A/C ratio obtained through experiments in this study are shown in Equations (4)–(6).

$$SA = 886.06PO + 188.24 \tag{4}$$

$$SA = 1066.8PO + 61.468 \tag{5}$$

$$SA = 1064.9PO - 75.809 \tag{6}$$

in which, SA: energy spectrum signal intensity; PO: porosity;

Therefore, the conversion of the T_2 energy spectrum curve measured by NMR to the pore size distribution map can be easily obtained by combining the relationship between pore radius and relaxation time as well as the relationship between energy spectrum signal intensity and porosity.

3.4.5. Fractal Model

It has been proved that the pore structure of cement-based porous materials has fractal characteristics. The complexity of pore structure will be well characterized using an appropriate fractal model, which serves as a representative parameter of pore structure characteristics [15]. Box dimension is one of the most widely-used dimensions, and its mathematical expression is as follows: let F be any nonempty bounded subset of the set of real numbers, and N be the minimum number of boxes of size δ that cover the F set. Then the box dimension can be calculated by Equation (7) [16].

$$D = \lim_{\delta \to 0} \frac{\ln_\delta(F)}{\ln(1/\delta)} \tag{7}$$

The pore radius under a given relaxation rate is measured using a low-field NMR instrument. Supposing the pore in the CA mortar to be a regular spherical pore combined with the definition of box dimension, spherical boxes with n sizes are selected for measurement, wherein the size δ of the spherical box corresponds to the pore diameter r_i (i = 1,2,...,n), and it is used to cover all the pores with a size $\geq r_i$. To calculate the number of boxes, the pore with a size $>r_i$ is converted to that with a size of r_i using the equal volume principle, so that the number of converted pores with a size of r_i is obtained (N_{ci}), resulting in a set of data [r_1, N_{c1}], [r_2, N_{c2}], [r_n, N_{cn}]. The reciprocal of pore size and the number of converted pores are subjected to linear regression in double-logarithmic coordinates, and the corresponding box dimension can be obtained based on the slope of the regression line. The above model was established based on the pore volume, and the calculated box dimension reflected the pore volume distribution, so this model was called the pore volume fractal model, and the corresponding fractal dimension is called the pore volume fractal dimension. The above model is converted into a specific expression, as follows:

$$\ln N = D \ln(1/r) + C \tag{8}$$

where r is the pore size, N is the number of pores with a size $\geq r$, and D is the pore volume fractal dimension.

4. Results and Discussion

4.1. Evolution Law of Microstructure of CA Mortar

The microstructure of CA mortar was scanned and photographed by environmental SEM (Figures 1–7). As can be seen from Figures 1–3, the cement hydration products, asphalt, standard sand and pores in CA mortar were all uniformly distributed, the CA mortar displayed a loose and porous structure with cement hydration products as the continuous phase and asphalt as the dispersion phase, and no complex interface structure with unhydrated cement particles-cement hydration products-asphalt-sand-pores was found [17]. The hydration products such as flocculent or granular hydrated calcium silicate (C-S-H gel), roll-leaf-like calcium hydroxide (C-H) and cluster-like ettringite (AFt) could be observed inside the mortar, the pore structure was almost round, and blocky, flaky and needle-like hydration products could also be observed in some pores. There was a clear boundary between the asphalt film and other hydration products, as shown by the blue line in Figures 1b and 3c. The dispersed asphalt was discontinuously distributed in the space in the form of film sheet and wrapped on the surface of hydration products, sand and pores.

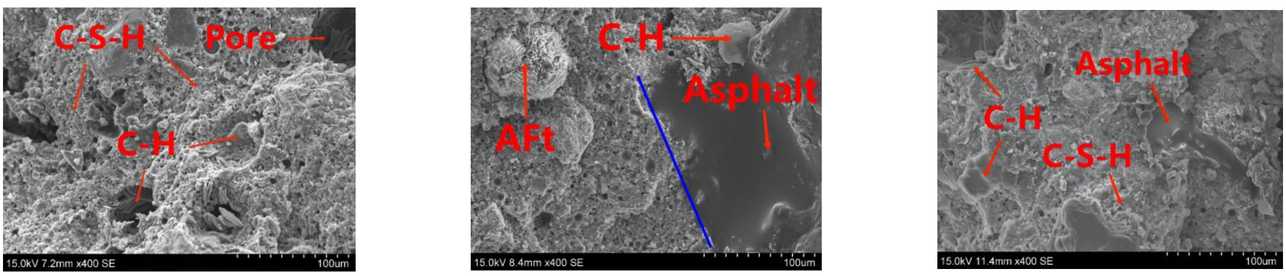

(**a**) (**b**) (**c**)

Figure 1. SEM images with the changes of curing ages (A/C = 0.4). (**a**) 7 d, (**b**) 14 d, (**c**) 28 d.

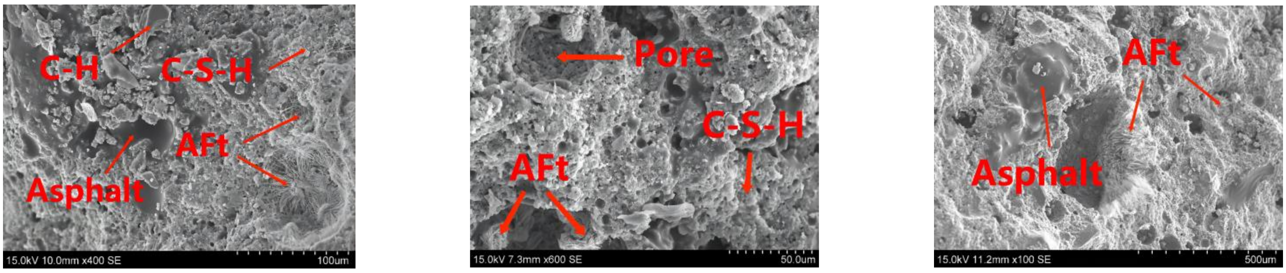

(**a**) (**b**) (**c**)

Figure 2. SEM images with the changes of curing ages (A/C = 0.5). (**a**) 7 d, (**b**) 14 d, (**c**) 28 d.

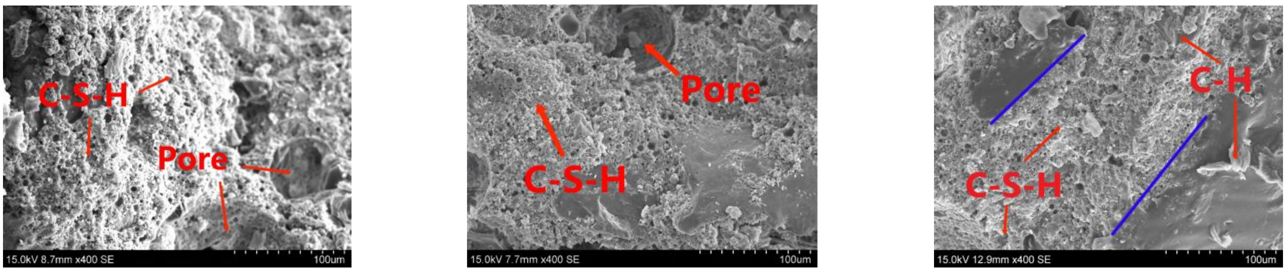

(**a**) (**b**) (**c**)

Figure 3. SEM images with the changes of curing ages (A/C = 0.6). (**a**) 7 d, (**b**) 14 d, (**c**) 28 d.

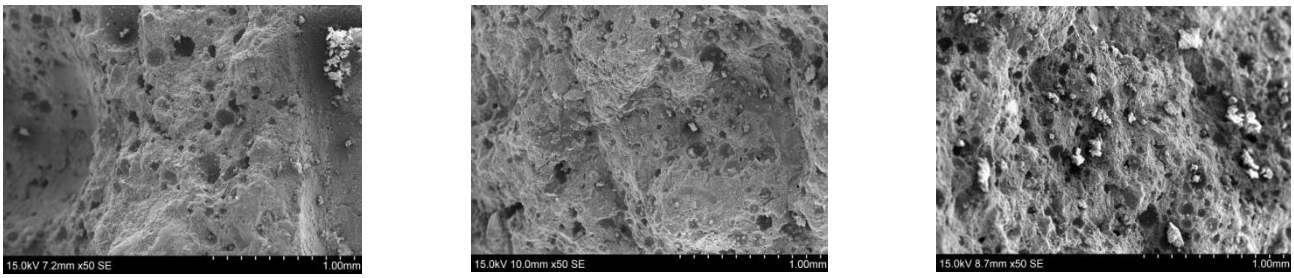

(**a**) (**b**) (**c**)

Figure 4. 7 d SEM images with the changes of A/C. (**a**) A/C = 0.4, (**b**) A/C = 0.5, (**c**) A/C = 0.6.

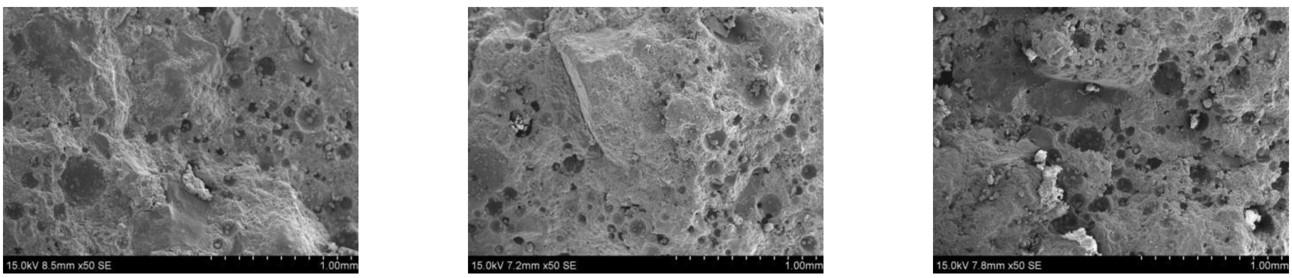

(**a**) (**b**) (**c**)

Figure 5. 14 d SEM images with the changes of A/C. (**a**) A/C = 0.4, (**b**) A/C = 0.5, (**c**) A/C = 0.6.

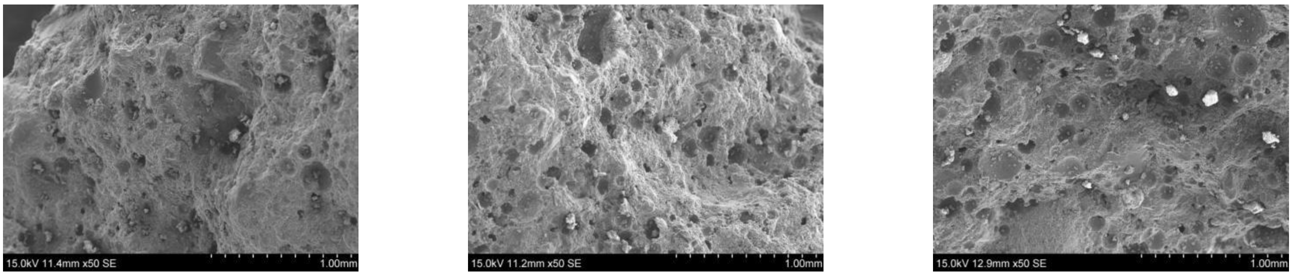

(**a**) (**b**) (**c**)

Figure 6. 28 d SEM images with the changes of A/C. (**a**) A/C = 0.4, (**b**) A/C = 0.5, (**c**) A/C = 0.6.

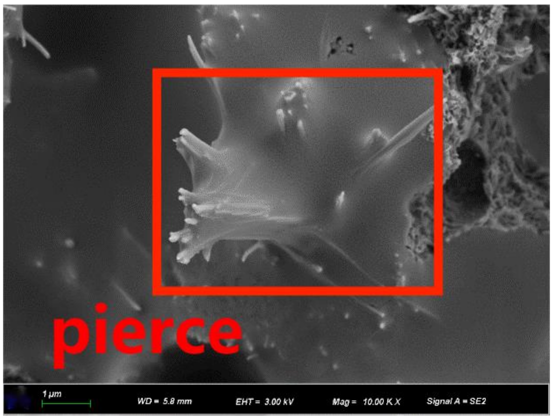

Figure 7. The hydration product punctures the asphalt film.

At the beginning of curing, there were some C-S-H and C-H as well as some pores in the CA mortar with different A/C ratios. With the increase in the curing age, more C-S-H, C-H and AFt were formed by cement hydration [18], which increased continuously and filled in the pore structure. As a result, the pores gradually shrank and decreased, asphalt gradually demulsified and chelated with hydration products, the pore wall became smoother, and the whole mortar became denser with optimized pore structures.

As shown from the SEM images (50×) in Figures 4–6, at the same curing age, with the increase in the A/C ratio, the overall pore density of mortar increased gradually, and the number of macro pores rose, and the pore structure became looser. The main reason is that with the decrease in cement dosage, the filling of the space structure by hydration products is reduced, so the pore structure becomes loose [19–24]; moreover, the water content of emulsified asphalt in the mortar is consumed continuously during the demulsification process, and the asphalt is gradually gathered, thus leaving pores. Therefore, the increase in the emulsified asphalt content will lead to more pores. At the same time, it can be seen from Figures 7 and 8 that more asphalt is wrapped and attached to the surface of cement particles and hydration products, hindering the hydration of cement, and gradually reducing the hydration products, which weakens the filling of the pore structure, thus increasing the overall pore density of mortar, and resulting in a looser pore structure. The above analysis demonstrates that the A/C ratio is an important influencing factor for the formation and evolution of CA mortar pore structure.

4.2. Evolution Law of Pore Size Distribution of CA Mortar

Based on the qualitative analysis of micro-pores of CA mortar by SEM, the pore structure of CA mortar was determined by NMR to further quantitatively study the pore structure of CA mortar.

The pore size distribution curves of CA mortar are shown in Figures 9 and 10. The results showed that the pore size distribution curves of CA mortar all presented a bimodal shape and the peak values were at 10–30 nm and 1000–4000 nm. The change in curing age and A/C ratio did not change the bimodal state of pore size distribution of mortar, but the position and size of peak value changed to a certain extent with the curing age and A/C ratio. With the increase in the A/C ratio and curing age, the first peak value declined, while the second peak value rose (the first peak and the second peak from left to right), and the most probable pore size gradually transferred from the first peak to the second peak [25,26].

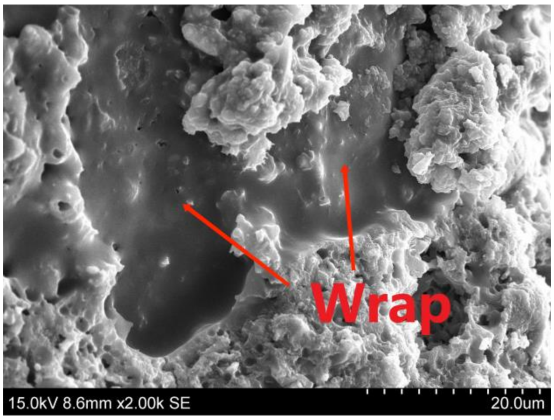

Figure 8. Asphalt coated on the surface of hydration products.

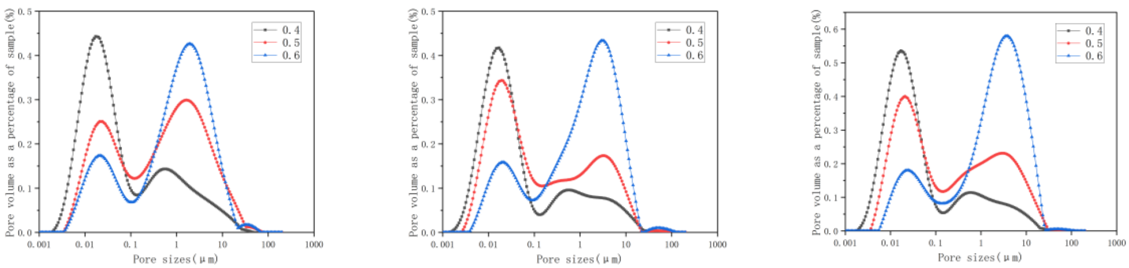

(**a**) (**b**) (**c**)

Figure 9. Comparison of pore radius distribution of mortars with different A/C ratios. (**a**) 7 d, (**b**) 14 d, (**c**) 28 d.

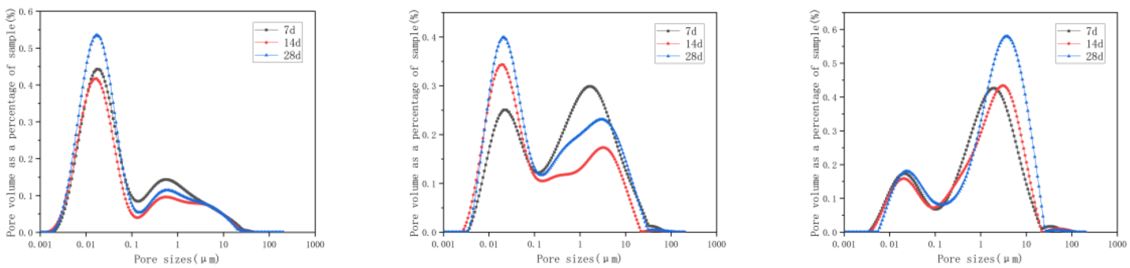

(**a**) (**b**) (**c**)

Figure 10. Changes in mortar pore radius distribution with curing age. (**a**) A/C = 0.4, (**b**) A/C = 0.5, (**c**) A/C = 0.6.

The pore structure classification principles adopted in this study are proposed by Butt: macro pores (d > 1000 nm), capillary pores (d = 100–1000 nm), transition pores (d = 10–100 nm) and gel pores (d < 10 nm) [27] The test data are presented in Table 2, the minimum and maximum probable pore sizes of CA mortar were 17 nm and 3823.29 nm, respectively, which were all distributed in the range of transition pores and macro pores. Meanwhile, with the increase in the curing age and A/C ratio, the mean pore size gradually declined.

Table 2. The pore structure parameters of CA mortar obtained by NMR analysis.

Specimen	Curing Age	The Total Porosity (%)	Probable Pore Sizes (nm)	The Mean Pore Size (nm)	The Pore Size Distribution (The Pore Size Distribution)			
					<10 nm (Gel Hole)	10–100 nm (Transition Hole)	100–1000 nm (The Capillary Hole)	>1000 nm (Macropore)
A/C = 0.4	7 d	9.19	17	1923.65	1.57	4.70	1.59	1.32
	14 d	8.00	17.01	1973.16	1.66	4.01	1.07	1.25
	28 d	8.65	17.01	1791.84	1.73	4.54	1.19	1.18
A/C = 0.5	7 d	16.12	1661.99	3355.48	0.89	5.16	4.09	5.97
	14 d	15.93	19.54	3467.72	1.76	6.75	2.99	4.42
	28 d	12.57	20.95	3070.65	0.71	4.06	2.88	4.92
A/C = 0.6	7 d	18.24	1909.54	3974.04	0.42	3.07	3.48	11.27
	14 d	16.99	3104.45	3769.01	0.53	2.90	3.85	9.71
	28 d	16.94	3823.29	3560.33	0.33	3.43	4.04	9.14

As shown in Figures 11 and 12, the change law of CA mortar was consistent with the increase in the A/C ratio at each curing age, i.e., the total porosity increased, the pore volume proportion of gel pores and transition pores decreased gradually, and the pore volume proportion of capillary pores and macro pores increased gradually. It can be seen that with the increase in the A/C ratio, the pore structure became looser, consistent with the results of SEM qualitative analysis. Therefore, the combination of the two test methods can characterize the pore structure of CA mortar more comprehensively, qualitatively and quantitatively.

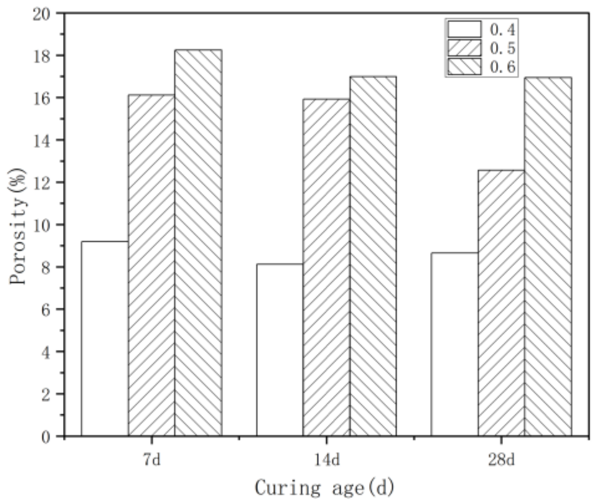

Figure 11. Comparison of porosity of CA mortar.

When the A/C ratio was the same, the total porosity showed a downward trend, the pore volume proportion showed a gradual decreasing trend for macro pores, and it had different changes for other pore types with the increase in the curing age. According to the SEM results in Figures 1–3, the cement hydration products gradually increased, the pore structure was continuously filled and refined, and the macro pores gradually evolved to the pores with a smaller size with the progress of curing, so the pore volume proportion of macro pores gradually decreased [28]. The reason the pore volume proportion had different changes for other pore types is that the cement hydration at the initial curing stage also promotes the continuous demulsification of emulsified asphalt. As shown in Figure 8, the dispersed asphalt particles were continuously gathered, filling some pore structures, so that the water could not enter, and NMR failed to identify the closed pores in this part. With the increase in the curing age, the hydration products from further hydration punctured the closed pores, so the closed pores were opened again and detected by NMR (Figure 7). At the same time, the further demulsification process might also lead to the migration of asphalt to reshape the pore structure, so the pore volume proportion in some pore-size ranges fluctuated, and the pore size distribution changed irregularly with the curing age.

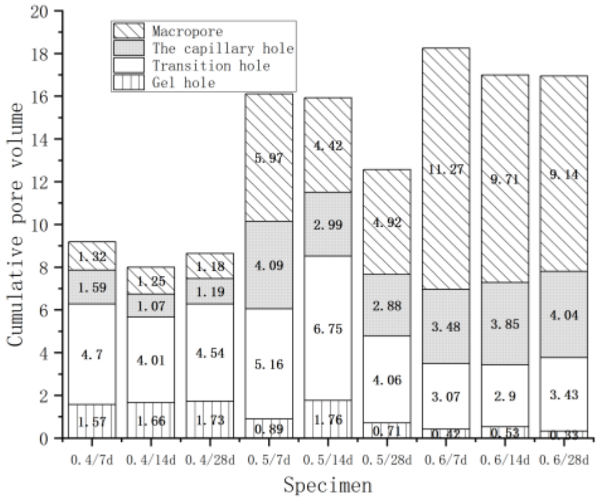

Figure 12. Porosity of various types of pores of CA mortar.

It can be seen that the content of asphalt is an important influencing factor for the pore structure evolution of CA mortar. The results of NMR and analysis reflected the change law of pore structure of CA mortar more quantitatively.

4.3. Fractal Characteristics of CA Mortar

Based on the NMR data of pore size distribution, the data were processed using the fractal model proposed in this study. The log-log scatter plots of the number of boxes and the reciprocal of the radius of CA mortar were plotted and subjected to fit by Equation (8). As shown in Figures 13–15, the goodness-of-fit obtained after fitting was all high (>0.99), suggesting that the pore structure of CA mortar has obvious fractal characteristics and conformed to the pore volume fractal model based on the box fractal model proposed in this study.

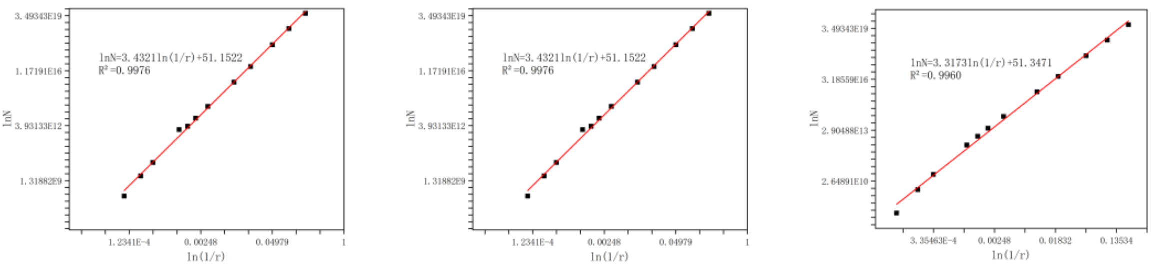

(**a**) (**b**) (**c**)

Figure 13. Log-log scatter plots of the number of boxes and the reciprocal of the radius of CA mortar at curing age of 7 d. (**a**) A/C = 0.4, (**b**) A/C = 0.5, (**c**) A/C = 0.6.

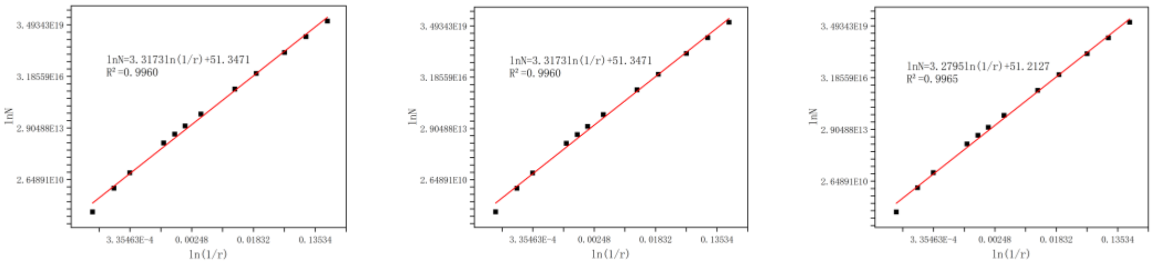

(**a**) (**b**) (**c**)

Figure 14. Log-log scatter plots of the number of boxes and the reciprocal of the radius of CA mortar at curing age of 14 d. (**a**) A/C = 0.4, (**b**) A/C = 0.5, (**c**) A/C = 0.6.

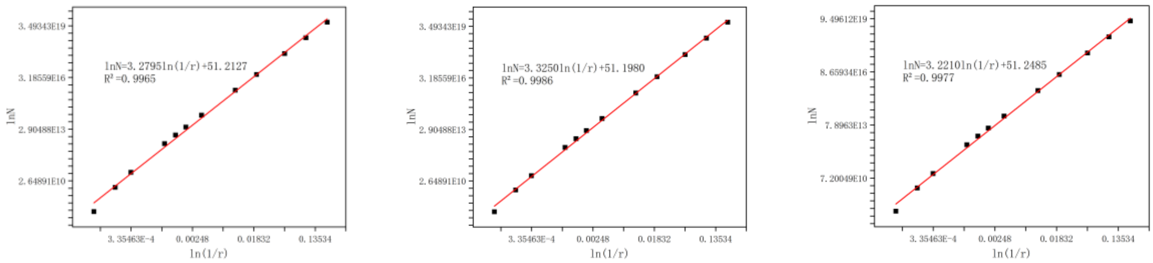

(**a**) (**b**) (**c**)

Figure 15. Log-log scatter plots of the number of boxes and the reciprocal of the radius of CA mortar at curing age of 28 d. (**a**) A/C = 0.4, (**b**) A/C = 0.5, (**c**) A/C = 0.6.

The volume fractal dimension and goodness-of-fit of CA mortar are listed in Table 3. It can be seen that the pore volume fractal dimension of CA mortar was >3, in line with the basic concept that the volume fractal dimension is generally >3 [29]. At the same curing time, the pore volume fractal dimension decreased with the increase in the A/C ratio, suggesting that the complexity of pore structure decreases.

Table 3. Fractal dimension of pore volume of CA mortar.

Specimen	**Curing Age**					
	7 d		**14 d**		**28 d**	
	D	**R^2**	**D**	**R^2**	**D**	**R^2**
A/C = 0.4	3.4321	0.9976	3.4302	0.9988	3.4696	0.9987
A/C = 0.5	3.3181	0.9979	3.3714	0.9980	3.3250	0.9986
A/C = 0.6	3.3173	0.9960	3.2795	0.9965	3.2210	0.9977

The correlation analysis was conducted between the pore volume fractal dimension and the interval porosity (Table 4). It was found that the fractal dimension was in strong positive correlation with gel pores, and in strong negative correlation with capillary pores and macro pores, i.e., the higher the proportion of pores with a small pore size and the larger the fractal dimension, the more complex the pore structure. This is consistent with the change law obtained from the pore size distribution curve, so the pore volume fractal dimension can quantitatively characterize the pore size distribution of CA mortar pore structure.

Table 4. Correlation coefficient between pore volume fractal dimension and interval porosity of CA mortar.

	Gel Hole	Transition Hole	The Capillary Hole	Macropore
Pearson-related	0.89833	0.41668	−0.92235	−0.86963
p-value	9.98×10^{-4}	0.26457	3.98×10^{-4}	0.00231

Note: The correlation between the *p* value at the 0.05 level is significant.

4.4. Relationship between Strength and Pore Structure of CA Mortar

The compressive and flexural strength test results of CA mortar with three kinds of mix proportions at different ages are shown in Figures 16 and 17. At the same curing age, with the increase in the A/C ratio, the compressive and flexural strength of CA mortar gradually decreased. Based on the above micro-analysis, it was found that the increase in A/C decreased the cement content and increased the asphalt content. As the strength of CA mortar mainly came from the cement hydration products, the hydration products had less filling for the space structure, failing to form an effective continuous phase [30]. Second, with the increase in the proportion of emulsified asphalt, cement hydration was hindered, and the cement hydration rate decreased [31]. Therefore, the strength of CA mortar decreased due to a decrease in cement hydration products and hydration rate.

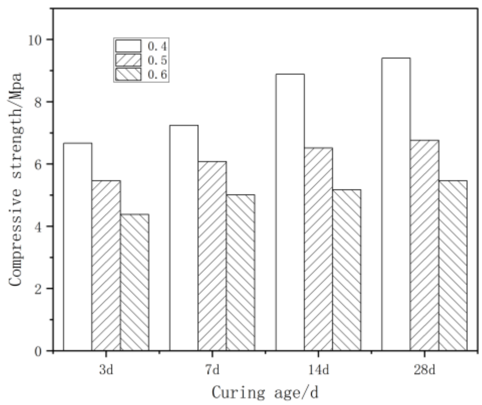

Figure 16. Compressive strength of CA mortar.

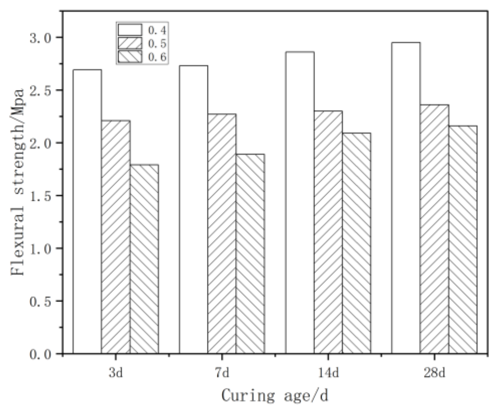

Figure 17. Flexural strength of CA mortar.

With the increase in the curing age, the compressive and flexural strength of CA mortar gradually increased. The reason is that with the increase in the curing age, cement hydration continued, cement hydration products gradually increased and filled the pore, emulsified asphalt gradually demulsified and filled the space structure with the hydration products, and the space structure gradually became dense, gradually enhancing the strength [32–34].

The purpose of studying the micro-pore structure is to establish the relationship between the micro-pore structure and the macro-properties, so as to reveal the micro-mechanism of the macro-properties and put forward the regulation and control methods of the macro-properties from a microscopic angle. Therefore, the compressive and flexural strength together with fractal dimension was subjected to regression analysis (Figures 18 and 19). Meanwhile, the compressive and flexural strength was subjected to correlation analysis with fractal dimension and interval porosity (Tables 5 and 6). It can be seen that the compressive and flexural strength was positively correlated with the fractal dimension, i.e., they increased with the increase in the fractal dimension, with correlation coefficients of 0.8713 and 0.8574, respectively. The fractal dimension is used to describe the complexity of the research object. From the definition of fractal dimension, it can be seen that the larger the fractal dimension, the higher the complexity of the described object, the pore structure distribution is more reasonable [29]. Therefore, the larger the fractal dimension, the more complex the pore structure will be, the higher the strength of the object. Therefore, a positive correlation can be observed between the strength of CA mortar and fractal dimension. The compressive and flexural strength had certain correlations with gel pores, capillary pores and macro pores, and the compressive and flexural strength increased with the increase in the proportion of gel pores, and decreased with the increase in the proportion of capillary pores and macro pores. Obviously, fractal dimension can be used as a comprehensive characterization parameter of pore size distribution, instead of multiple parameters of interval pore volume, to establish a relationship model between strength and pore structure, thereby providing a basis for improving the macro-properties of CA mortar from the microstructure.

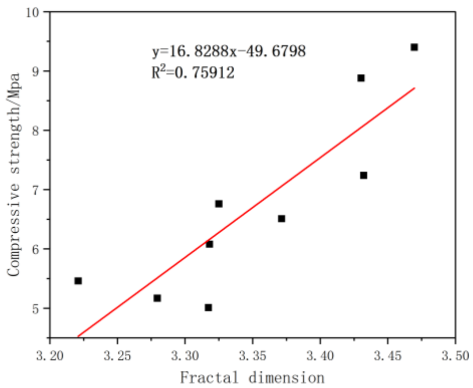

Figure 18. Regression relationship between compressive strength (Cs) and fractal dimension of CA mortar.

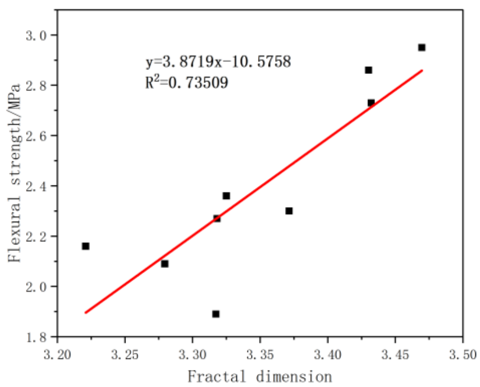

Figure 19. Regression relationship between flexural strength (Fs) and fractal dimension of CA mortar.

Table 5. Correlation coefficient of compressive strength and fractal dimension and interval porosity of CA mortar.

	Fractal Dimension	Gel Hole	Transition Hole	The Capillary Hole	Macropore
Pearson-related	0.87127	0.8121	0.30419	−0.9141	−0.90933
p-value	0.00222	0.00784	0.42613	5.62×10^{-4}	6.76×10^{-4}

Note: The correlation between the *p* value at the 0.05 level is significant.

Table 6. Correlation coefficient of flexural strength and fractal dimension and interval porosity of CA mortar.

	Fractal Dimension	Gel Hole	Transition Hole	The Capillary Hole	Macropore
Pearson-related	0.85737	0.81728	0.30326	−0.9117	−0.95109
p-value	0.00313	0.00715	0.42762	6.17×10^{-4}	8.12×10^{-5}

Note: The correlation between the *p* value at the 0.05 level is significant.

5. Conclusions

The morphology of pore structure and pore size distribution of CA mortar were explored in this study. The evolution laws of the microstructure and pore size distribution of CA mortar with the A/C ratio and curing age were investigated by SEM and NMR. The main conclusions are as follows:

(1) The results of SEM showed that the microscopic morphology of CA mortar mainly presents a loose and porous space structure with cement hydration products being the continuous phase and asphalt being the dispersed phase, suggesting that CA mortar is a typical porous material.
(2) With the increase in A/C ratio, the total porosity and average pore size of CA mortar gradually increase. This may be due to the hydration products produced by cement hydration decrease, and the increase in the amount of asphalt hindering the hydration process of the cement. With the increase in curing age, cement hydration products developed and filled the pores in CA mortar, which made the pore structure of CA mortar more compact and the porosity decreased. However, due to the influence of asphalt, the evolution law of CA mortar pore structure with age is not consistent under different A/C ratios.
(3) A fractal model of CA mortar pore volume was proposed based on the concept of box fractal dimension and the experimental data of NMR, the pore structure of CA mortar was proved to have obvious fractal characteristics. The correlation analysis proves that the fractal dimension of the pore volume of CA mortar has an positive correlation with the compressive and flexural strength, which suggest that fractal dimension of pore volume can be a bridge for connecting the macro-property and micro-structures of CA mortar.

Author Contributions: Supervision, S.J.; Writing—original draft, W.Z.; Writing—review & editing, Y.Z. All authors have read and agreed to the published version of the manuscript.

Funding: This research was funded by the National Key R&D Program of China (2021YFB2601200); The National Natural Science Foundation of China (52078024); R&D Program of Beijing Municipal Education Commission (KM202110016011).

Institutional Review Board Statement: Not applicable.

Informed Consent Statement: Not applicable.

Data Availability Statement: Not applicable.

Conflicts of Interest: The authors declare no conflict of interest.

References

1. Fu, Q.; Zheng, K.R.; Xie, Y.J.; Zhou, X.L.; Cai, F.L. Fractal Characteristics of Pore Volume of Cement Emulsified Asphalt Mortar. *J. Silic.* **2013**, *41*, 1551–1557.
2. Kong, X.M.; Zhang, Y.R.; Zhang, J.Y.; Ma, X.W.; Cao, E.X.; Liu, Y.L.; Huang, W.L. Study on Fluidity and Microstructure of Fresh Cement Asphalt Slurry. *J. Build. Mater.* **2011**, *14*, 569–575.
3. Li, W.; Zhu, W.T.; Shi, Y.L.; Hong, J.X.; Yang, D.Y. Effect of cationic emulsified asphalt on cement hydration and properties of CA mortar. *Concr. Cem. Prod.* **2020**, *12*, 1–5. [CrossRef]
4. Deng, D.H.; Ye, T.; Yuan, Q.; Wang, Y. Comparison of Pore Structure and Testing Methods of Cement Emulsified Asphalt Mortar. *J. Build. Mater.* **2016**, *19*, 933–938.
5. Yuan, Q.; Deng, D.H.; Wang, Y. Cement emulsified asphalt mortar for high-speed railway. *Sci. Bull.* **2020**, *65*, 2384–2394.
6. Li, C.J.; Sun, Z.P.; Li, Q.; Luo, Q. Application of low-field nuclear magnetic resonance technology in cement-based materials. *Mater. Rev.* **2016**, *30*, 133–138.
7. Liu, Z.Q.; Li, X.N.; Tian, Q.; Deng, D.H.; Yuan, Q. Microscopic analysis on the development of static mechanical properties of CRTS II cement emulsified asphalt mortar. *China Sci. Tech. Sci.* **2014**, *44*, 681–686.
8. Temporary Technical Conditions for Cement Emulsified Asphalt Mortar for CRTS II Slab Ballastless Track of Passenger Dedicated Railway. 2008. Available online: https://jz.docin.com/p-25301051.html (accessed on 25 August 2022).
9. *GB/T 17671-2021.2021-12-31*; Test Method for the Strength of Cement Mortar (ISO Method). China Building Materials Federation: Beijing, China. Available online: https://www.sosoarch.com/guifan/details.aspx?id=281 (accessed on 25 August 2022).
10. Yao, W.; She, A.M.; Yang, P.Q. 1H NMR relaxation characteristics and state evolution of evaporable water in cement slurry. *J. Silic.* **2009**, *37*, 1602–1606.
11. Wyrzykowski, M.; McDonald, P.J.; Scrivener, K.L.; Lura, P. Water Redistribution within the Microstructure of Cementitious Materials Due to Temperature Changes Studied with 1H NMR. *J. Phys. Chem. C* **2017**, *121*, 27950–27962. [CrossRef]
12. McDonald, P.J.; Gajewicz, A.M.; Morrell, R. 1H NMR characterisation of pore water in cement materials. In Proceedings of the 36th Cement and Concrete Science Conference, Cardiff, UK, 5–6 September 2016.
13. Wang, Y.; Yuan, Q.; Deng, D.; Ye, T.; Fang, L. Measuring the pore structure of cement asphalt mortar by nuclear magnetic resonance. *Constr. Build. Mater.* **2017**, *137*, 450–458. [CrossRef]
14. Cheng, H.C.; Liu, S.Q.; Hu, Z.Q. Regularity of rock pore disturbance evolution based on nuclear magnetic resonance (NMR) analysis method. *Water Electr. Energy Sci.* **2022**, *40*, 176–180. [CrossRef]
15. Zhang, Q.Z.; Fang, Y.; Song, L.; Xu, N.; Kang, Z.H. Pore structure of concrete and its fractal dimension and chloride ion diffusion performance relationship. *J. Silic. Bull.* **2022**, *9*, 2716–2727. [CrossRef]
16. Jiang, N. The historical evolution of the concept of box dimension. *J. Dialectics Nat. Res.* **2020**, *4*, 84–90. [CrossRef]
17. Wang, H.F. Study on mechanism, test and influencing factors of cement hydration process. *Chem. Ind. Manag.* **2015**, *26*, 191.
18. Zhu, Z.Y.; Wang, Z.P.; Zhou, Y.; Chen, Y.T.; Wu, K. Portland cement hydration products of micro-nano structure in situ study. *J. Silic.* **2021**, *49*, 1699–1705. [CrossRef]
19. Chen, Y. Study on pore size distribution of outburst coal sample. *Coal* **2019**, *28*, 55–62.
20. Harada, Y. Development and utility of grout for a track structure with grout filled ballast. *Q. Rep. RTRI* **1976**, *15*, 25–27.
21. Harda, Y.; Tottori, S.; Itai, N. Development of cement asphalt mortar for slab tracks in cold climate. *Q. Rep. RTRI* **1983**, *15*, 62–67.
22. Harada, Y. Development of Ultrarapid–Hardening Cement-asphalt Mortar for Grouted–Ballast Track Structure. *Q. Rep. RTRI* **1976**, *17*, 6–11.
23. Torii, O.; Mizunuma, T.; Mino, I.; Ando, T. Cement Asphalt Ballast Grout Composition for Track. U.S. Patent US3867161, 18 February 1975.
24. Higuchi, Y.; Harada, Y.; Sato, T. Quick Hardening Cement–Asphalt Composition. U.S. Patent US4084981, 18 April 1978.
25. Wang, C.P.; Zhang, J.S. Analysis on the development law of concrete porosity under sulfate erosion based on nuclear magnetic resonance technology. *Shandong Sci.* **2022**, *35*, 65–72+98.
26. Zhang, M.; Zhang, P.; Zhang, H.B. Pore structure of concrete material. *Sci. Technol. Inf.* **2007**, *36*, 139–140.
27. Zhu, L.; Jin, Q.; Hu, D. Analysis of pore Structure Characteristics of Steel slag-cement Composites Based on low field nuclear magnetic resonance Technique. *Compr. Util. Fly Ash* **2020**, *34*, 71–76.
28. Zhang, W.; Liu, C.; Liu, H.W.; Lin, X.; Zhang, Z.N. Deterioration mechanism of rice husk ash concrete based on Fractal dimension of pore volume. *J. Compos. Mater.* **2022**, *1–13*, 1–13. [CrossRef]
29. Li, Y.X.; Chen, Y.M.; He, X.Y.; Wei, J.X.; Zhang, W.S.; Zhang, H.T.; Guo, S.H. Fractal dimension of pore volume and its relationship with pore structure and strength in fly ash cement paste. *J. Chin. Ceram. Soc.* **2003**, *8*, 774–779.
30. Lin, H.; Cao, D.G.; Bai, X.K.; Lao, Z.M.; Zhu, J.Y.; Zeng, J.M. Characteristics of density and strength of hydration products of slag containing cement. *Sichuan Build. Mater.* **2020**, *46*, 39–41.
31. Tziotziou, M.; Karakosta, E.; Karatasios, I.; Diamantopoulos, G.; Sapalidis, A.; Fardis, M.; Maravelaki-Kalaitzaki, P.; Papavassiliou, G.; Kilikoglou, V. Application of 1H NMR to hydration and porosity studies of lime-pozolan mixtures. *Microp. Mesop. Mater.* **2011**, *139*, 16. [CrossRef]
32. Ozawa, H.; Murata, Y. Repair Method in Slab Type Track. WO 2008057318(A), 15 May 2008.

33. Hall, C. Water movement in porous building materials—I. Unsaturated flow theory and its application. *Build. Environ.* **1977**, *12*, 117–125. [CrossRef]
34. Hall, C. Water movement in porous building materials—VI. The sorptivity of mortars. *Build. Environ.* **1986**, *21*, 113–118. [CrossRef]